Predictions of local ground geomagnetic field fluctuations during the 7-10 November 2004 events studied with solar wind driven models

P. Wintoft, M. Wik, H. Lundstedt, L. Eliasson

Annales Geophysicae, 23, 3095–3101, 2005
SRef-ID: 1432-0576/ag/2005-23-3095

Annales Geophysicae

Predictions of local ground geomagnetic field fluctuations during the 7–10 November 2004 events studied with solar wind driven models

P. Wintoft[1], **M. Wik**[1], **H. Lundstedt**[1], **and L. Eliasson**[2]

[1]Swedish Institute of Space Physics, Lund, Sweden
[2]Swedish Institute of Space Physics, Kiruna, Sweden

Received: 22 February 2005 – Revised: 6 July 2005 – Accepted: 13 July 2005 – Published: 22 November 2005

Part of Special Issue "1st European Space Weather Week (ESWW)"

Abstract. The 7–10 November 2004 period contains two events for which the local ground magnetic field was severely disturbed and simultaneously, the solar wind displayed several shocks and negative B_z periods. Using empirical models the 10-min RMS ΔX and ΔY at Brorfelde (BFE, 11.67° E, 55.63° N), Denmark, are predicted. The models are recurrent neural networks with 10-min solar wind plasma and magnetic field data as inputs. The predictions show a good agreement during 7 November, up until around noon on 8 November, after which the predictions become significantly poorer. The correlations between observed and predicted log RMS ΔX is 0.77 during 7–8 November but drops to 0.38 during 9–10 November. For RMS ΔY the correlations for the two periods are 0.71 and 0.41, respectively. Studying the solar wind data for other L1-spacecraft (WIND and SOHO) it seems that the ACE data have a better agreement to the near-Earth solar wind during the first two days as compared to the last two days. Thus, the accuracy of the predictions depends on the location of the spacecraft and the solar wind flow direction. Another finding, for the events studied here, is that the ΔX and ΔY models showed a very different dependence on B_z. The ΔX model is almost independent of the solar wind magnetic field B_z, except at times when B_z is exceptionally large or when the overall activity is low. On the contrary, the ΔY model shows a strong dependence on B_z at all times.

Keywords. Magnetospheric physics (Solar wind-magnetosphere) – Geomagnetism and Paleomagnetism (Rapid time variations) – Ionosphere (Modeling and forecasting)

1 Introduction

The Earth's magnetosphere is a dynamic system that responds to changes in the upstream solar wind. Through complex processes that includes magnetic reconnection and viscous instabilities, energy is transferred from the solar wind into the magnetosphere (Baumjohann and Haerendel, 1987), with subsequent energy dissipation through geomagnetic storms and substorms (Gonzalez et al., 1994). A major fraction of large geomagnetic storms is caused by coronal mass ejections (CME) (Gosling et al., 1991). The CME, and its interplanetary counterpart, the ICME, plows through the ambient solar wind, producing shock waves and following sheath regions (Owens et al., 2005). In some cases the ICME evolves as a magnetic cloud (Burlaga, 1995) with smooth magnetic field line rotation during which the B_z component may be strongly negative for an extended period of time, enabling entry of solar wind energy through magnetic reconnection. Another source for geomagnetic activity, especially during the declining phase of solar activity, is seen in high speed solar wind streams (Richardson et al., 2002). The different structures interact and evolve as they travel from the Sun to the Earth, causing various degrees of geoeffectiveness (Huttunen et al., 2002; Echer and Gonzales, 2004).

During the geomagnetic storm, different current systems are modified, like the ionospheric currents, ring current, and magnetopause current. On the ground the currents are observed as deviations of the local geomagnetic field (Nishida, 1978). Several indices have been derived for various geophysical phenomena (Mayaud, 1980) and their coupling to the solar wind have been extensively studied (Baker, 1986), and especially the D_{st} index (Wu and Lundstedt, 1997; Klimas et al., 1998). The effects of geomagnetic disturbances are observed on technological systems, such as electrical power grids, pipe lines, and telegraph lines (Boteler et al., 1998, Lundstedt, 2004[1]), and are called geomagnetically

Correspondence to: P. Wintoft
(peter@lund.irf.se)

[1]Lundstedt, H.: The Sun, Space Weather and GIC Effects in Sweden, Adv. Space Res, in review, 2004.

induced currents (GIC). There is great interest in modelling GIC, both for post-event analysis and for predictions. As a result there are three parallel GIC studies within the ESA Space Weather Applications Pilot Project and these can be found at the web page http://www.esa-spaceweather.net/.

The GIC can be estimated in different ways. One approach is to use geomagnetic indices, as several can be successfully predicted: AE (Gleisner and Lundstedt, 2001a), D_{st} (Vassiliadis and Klimas, 1999; Lundstedt et al., 2002), and K_p (Boberg et al., 2000). The index is then translated into a physical quantity that is related to GIC. Boteler (2001) showed that there is close to a linear relationship between the 3-h K_p index and the logarithm of the ground electric field. However, the indices have their limitations because they have been derived to capture some specific aspect of the magnetospheric variation. Another approach is to use observed ground geomagnetic field data. The calculation of GIC can then be divided into two steps (Pirjola, 2002) involving a geophysical part to determine the geoelectric field and an engineering part to compute the currents in the technological system. The electric field is computed from the magnetic field by assuming an equivalent ionospheric current system such that the geomagnetic variations at the Earth's surface can be explained by horizontal divergence-free ionospheric currents (Viljanen et al., 2003). Solar wind–magnetosphere coupling models can then be used to predict the local ground magnetic field. In Gleisner and Lundstedt (2001b) a model was developed that predicts the 10-min average local geomagnetic field using solar wind data. But, as the electric field is related to the rate-of-change of the magnetic field (dB/dt) via Faraday's law of induction $\nabla\times E=-\frac{\partial B}{\partial t}$, a more basic quantity to use is the time difference of B, i.e. $\Delta B(t)=B(t+1)-B(t)$ (Viljanen et al., 2001). However, most of the power in ΔB is located at small scales (high frequencies) and therefore a large fraction of the signal will be lost if ΔB is temporally averaged, or if ΔB is formed from a temporally averaged B (Wintoft, 2005). This happens already at 5 to 10 min averages. Therefore, other moments of ΔB should be considered. In the work by Weigel et al. (2002) models were developed that predict the average absolute value of ΔB with a temporal resolution of 30 min. More specifically, they studied the north-south component of the magnetic field, i.e. $\langle|\Delta X|\rangle_{30\mathrm{min}}$. As the average is taken of the absolute value, a large fraction of the variance from the original signal is maintained. The best model reached an overall prediction efficiency of 0.4 based on data from 1998–1999.

The models developed by Wintoft (2005) aims instead at predicting the 10-min root-mean-square (RMS) of ΔX (and ΔY). The motivation of using RMS data is summarised here. The power spectrum of ΔX peaks at small scales and decreases quickly with increasing scale: 83% of the power is located at scales $\tau\leq 8$ min, 99% at $\tau\leq 128$ min. We speak in terms of scales as defined from wavelet analysis, but the scale may be translated into the approximate frequency band $[1/4\tau, 1/2\tau]$ (Percival and Walden, 2002). One may also picture the signal at a certain scale as being the difference between two consecutive averages of width τ. It was found that the RMS data can be used to estimate the power spectra of ΔX and ΔY. This is useful for the subsequent analysis, for example, computing GIC, as both amplitude and scale (frequency) are available. Another issue is that the RMS data captures a major fraction of the variance in ΔX. The relative variance is $\mathrm{Var}(\mathrm{RMS}\Delta X)/\mathrm{Var}(\Delta X)=0.82$. For comparison the 10-min average absolute ΔX has a relative variance of $\mathrm{Var}(\langle|\Delta X|\rangle)/\mathrm{Var}(\Delta X)=0.55$. Finally, any temporal averaging will decrease the forecast lead time. To illustrate this we may consider a time dependent parameter $x(t)$ that is collected with a sampling interval Δt that results in the time series x_i. The corresponding time stamp t_i marks the beginning of the interval so that x_i is the average of $x(t)$ over the interval $t\in[t_i, t_{i+1}]$, where $t_{i+1}=t_i+\Delta t$. Similarly, we may have another variable $y(t)$ sampled to y_i. If we now wish to develop a model that predicts y from x with lead time T we have $\hat{y}(t+T)=f(x(t))$, where $\hat{y}$ is the prediction of y. This leads to the discrete model $\hat{y}_{i+k}=f(x_i)$ where $T=k\Delta t$. Now assume that the current time is t_0. The latest available input is x_{-1} and it has been collected over the time interval $[t_{-1}, t_0]$. With a forecast time of $T=k\Delta t$ we will therefore forecast y_{k-1}, resulting in a true forecast time of $T'=T-\Delta t$. In order for the model to perform actual forecasts, we must have $\Delta t\leq T$.

In this work we will use the previously developed models to predict the disturbed period during 7 to 10 November 2004. The following section describes the observed data, Sect. 3 describes the model, Sect. 4 address forecast errors related to the location of the solar wind monitor and the control of the IMF B_z component. In Sect. 5 the conclusions are given.

2 The 7–10 November 2004 events

The 7–10 November 2004 period contains two events for which the local ground magnetic field was severely disturbed and the solar wind displays several shocks and negative B_z periods. In Fig. 1 the solar wind plasma and magnetic field data are shown, together with the ground magnetic field deviations at Brorfelde (BFE, 11.67° E, 55.63° N). The deviations are the one-minute differences of the north-south (X) and east-west (Y) magnetic field components

$$\Delta X(t) = X(t+1) - X(t), \tag{1}$$

$$\Delta Y(t) = Y(t+1) - Y(t), \tag{2}$$

as approximations to dX/dt and dY/dt. The solar wind data comes from three spacecraft: ACE (blue line), WIND (green line), and SOHO (red dots). The ACE (Smith et al., 1998; McComas et al., 1998) and WIND (Ogilvie et al., 1995) data have been resampled to 10-min averages while the SOHO (Ipavich et al., 1998) data are one-hour averages. The four top panels show the particle density n, the standard deviation σ_n of the density, the B_z magnetic field component in GSM, and the velocity V. The next two panels show the one-minute differences ΔX and ΔY. The two panels also contain the

10-min root-mean-square (RMS) of ΔX and ΔY. The bottom panel shows the north-south magnetic field X, minus 17 150 nT, and the D_{st} index. The five vertical lines indicates the times of solar wind shocks. It is clear that these shocks are followed by sudden increases in $|\Delta X|$ and $|\Delta Y|$. As the geomagnetic storm develops, large variations in ΔX and ΔY are seen. During 8 November, the extreme values reach (ΔX, ΔY)=(140, 116) nT/min and during 9 November (ΔX,ΔY)=(-242, -229) nT/min. The corresponding 10-min RMS extreme values are (96,61) nT/min and (122, 104) nT/min, respectively. We also note that the ratio RMSΔX/RMSΔY decreases from 1.6 for 8 November event to 1.2 for the 9 November event, indicating that the disturbance is more along the north-south direction during the first event. These events have not yet been described in the scientific literature, however, a description can be found at Space Environment Center (http://www.sec.noaa.gov/weekly/).

We see that the Sun was very active with several CMEs. The first shock in early 7 November was probably caused by a CME on 3 November. There was a small increase in the solar wind magnetic field with a negative B_z component. Both ΔX and ΔY display an impulse 66 min later in accordance with the ACE-magnetopause travel time of $t_{\rm ACE}$=68 min at the velocity of 365 km/s. The second shock, caused by a CME on 4 November was accompanied with larger increases in particle density n, σ_n, and B. B_z turned initially northward and later southward. The shock was followed by a magnetic impulse 55 min later, again in agreement with the 420 km/s velocity ($t_{\rm ACE}$=59 min). Both ΔX and ΔY continued to be slightly disturbed and D_{st} showed a weak increase followed by a weak decrease typical for the magnetic storm initial and main phases. At the third shock the velocity jumped from 500 km/s to above 650 km/s, the magnetic field increased to almost 50 nT and B_z turned initially northward and later strongly southward for an extended period of time. The source for this event was probably a series of CMEs that occurred late on 4 and early 6 November. The magnetic impulse took place 33 minutes later, in good agreement with a velocity of 650 km/s ($t_{\rm ACE}$=38 min). The disturbed period continued for about 19 h and D_{st} reached -373 nT on 8 November. What looks like a magnetic impulse early in 9 November is most likely a spurious value, as there are data gaps around that point and other stations show no such feature. The fourth shock, around noon on 9 November shows quite different velocities for ACE/WIND and SOHO. The magnetic impulse occurs 16 min after the shock and is similar in strength to that after the second shock. With a velocity of $V_{\rm ACE}$=790 km/s there should be a delay of $t_{\rm ACE}$=32 min. It is thus difficult to associate this magnetic impulse with the measured solar wind at ACE. The fourth shock shows a jump in velocity from 650 km/s to 800 km/s and a magnetic impulse follows 29 min later, in agreement with $t_{\rm ACE}$=31 min.

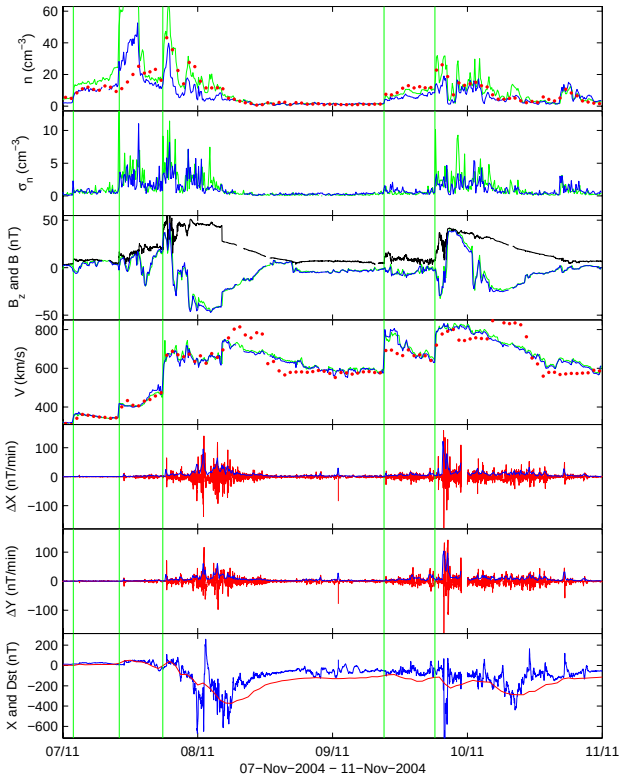

Fig. 1. The panels show, from top to bottom: solar wind density n (ACE–blue, WIND–green, SOHO–red), standard deviation σ_n of the density, B_z magnetic field component in GSM and total field B from ACE (black), velocity V, one-minute ΔX (red) and 10-min RMS ΔX (blue), one-minute ΔY and 10-min RMS ΔY, and one minute X (blue) and hourly D_{st} (red). The period extends over the four days of 7–10 November 2004. The only available data from SOHO are the hourly average density and velocity.

3 Forecasting RMS (ΔX,ΔY) using ACE

The empirical models previously developed predict the 10-min RMS ΔX and ΔY for southern Scandinavia, with a prediction lead time of 30 min (Wintoft, 2005). The models are recurrent neural networks with solar wind plasma and magnetic field data as inputs: 10-min averages of magnetic field B_z, particle density n, velocity V, and standard deviations (σ) of the same parameters. Local time and time of year were also used.

The models were trained and validated on data from the six year period 1998–2003. As the distributions of RMS ΔX and ΔY are dominated by values close to zero only a selected subset was used, in order to avoid the network becoming biased towards quiet conditions. However, large values are still typically underestimated, as they are more infrequent. The prediction horizon of 30 min was selected to enable the models to predict events with a large range of solar wind velocities. A velocity of 830 km/s at L1 takes 30 min to reach the magnetopause. We also studied models where the prediction lead time was increased up to 90 min, but for both ΔX and ΔY the correlation decreased. A large set of neural

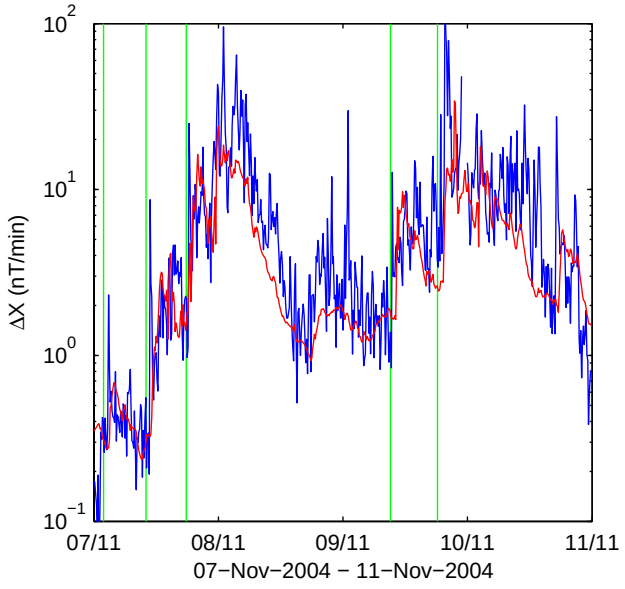

Fig. 2. The figure shows the observed (blue) and predicted (red) 10-min RMS ΔX.

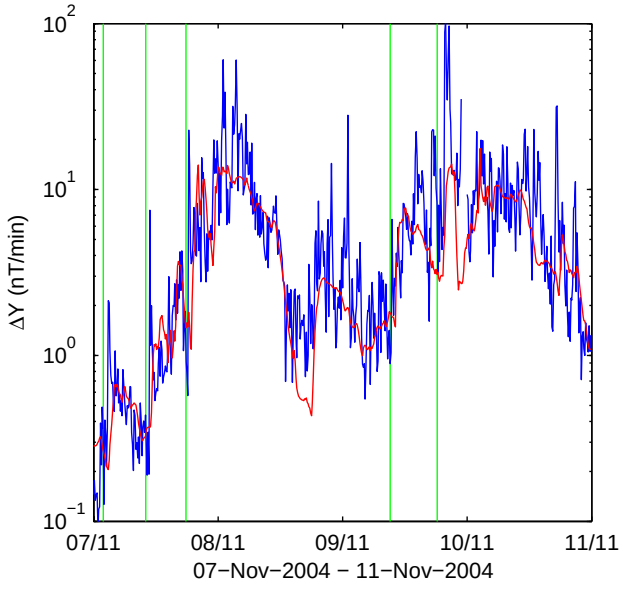

Fig. 3. The figure shows the observed (blue) and predicted (red) 10-min RMS ΔY.

networks were trained and the optimal models gave a correlation of 0.79 and prediction efficiency (Detman and Vassiliadis, 1997) of 0.63 of the logarithm of the RMS data. It is important to notice here that the geomagnetic data are not used as input to the model, only solar wind data, otherwise the correlation could be even higher but not necessarily truly improving the predictions. For example, a simple persistence model, predicting RMS $\Delta X(t+30\,\text{min})$ based on RMS $\Delta X(t)$, would have a correlation of 0.72 but the predictions would consistently lag by 30 min. To verify that the solar wind–ΔX model is actually making 30 min forecasts, with the stated correlation, we may compute the correlation coefficient between the observed ΔX and the predicted ΔX by shifting the predicted ΔX backwards and forwards in time. For a true forecast the maximum correlation should occur at 30 min and decrease for smaller and larger prediction times, and this is also the case for the neural network models.

It was shown that the solar wind influence on ΔX and ΔY were slightly different. The most important inputs for ΔX, in order of increasing importance, were local time, B_z, σ_n, and V. For ΔY it was local time, σ_n, V, and B_z. The other inputs, and mots notably n, had no significant influence. The independence of n was also shown by Weigel et al. (2002). The models have been implemented for real time operation and the forecasts are displayed on a web page (http://www.lund.irf.se/gicpilot/gicforecastprototype/). The predictions of RMS ΔX and ΔY for the November events are shown in Figs. 2 and 3. It is seen that the predictions capture the large-scale variations but not the sample-to-sample variations. The predictions show a good agreement during 7 November, up until around noon on 8 November, after which the predictions become significantly poorer. The correlations between observed and predicted log RMS ΔX is 0.77 during 7–8 November but drops to 0.38 during 9–10 November. For RMS ΔY the correlation for the two periods are 0.71 and 0.41, respectively.

4 Discussion

In the following sections we address the forecast quality in relation to the location of the solar wind monitor and study the coupling to the solar wind B_z component.

4.1 The locations of solar wind monitors

The ACE spacecraft is in orbit around L1 approximately 240 Earth radii (R_E) upstream from Earth. Due to the large distance there may be considerable differences in solar wind properties at ACE and close to Earth. In the study by Dalin et al. (2002) it was shown that the correlation of solar wind plasma data from different spacecraft could, at times, be small and the correlation decreased with increasing (Y,Z)-separation. For the period studied here the ACE spacecraft is located approximately at (X,Y,Z)=(242, 23, −15) R_E in GSE coordinate system. Two other spacecraft are also located around L1, namely SOHO at (218, −104, −3) R_E and WIND at (199, 59, −9) R_E. The spacecraft are almost located in the (X,Y)-plane, with the largest separation of 12 R_E in the Z-direction. However, in the Y-direction the distance is as large as 163 R_E. In the X-direction the separation is about 42 R_E, and with a velocity of 400 km/s or higher the separation in time is less than 11 minutes. From Fig. 1 we see that the B_z magnetic field components for ACE and WIND are very well correlated. There is a shift of $<$10 min, barely visible in the figure, that comes from the separation in X. Studying the velocity, there is again a very good agreement between ACE

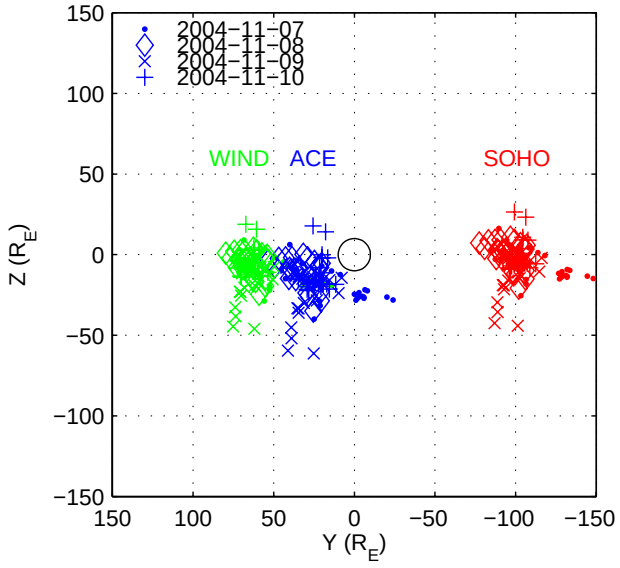

Fig. 4. The figure shows the advected spacecraft locations onto the plane X=10 R_E using hourly average velocity vectors from WIND. The data have been divided into the four days: 7 November (dots), 8 November (diamonds), 9 November (crosses), and 10 November (pluses). The black circle is centred on Earth and has a radius of 10 R_E.

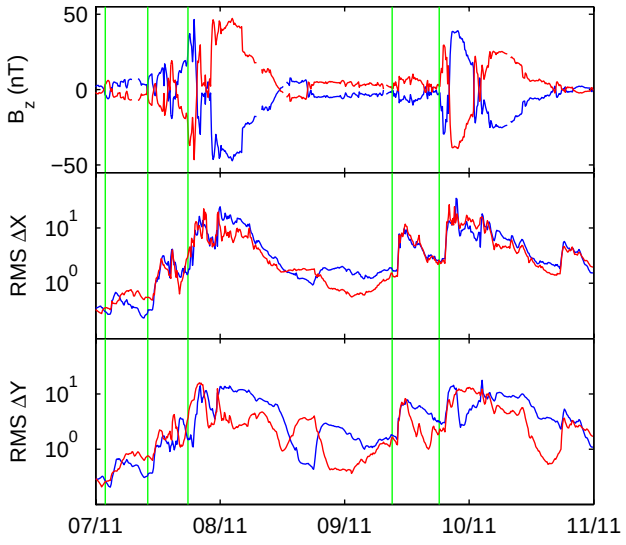

Fig. 5. The three panels show, from top to bottom: solar wind B_z (blue) and $-B_z$ (red), predicted RMS ΔX using B_z (blue) and $-B_z$ (red), and predicted RMS ΔY using B_z (blue) and $-B_z$ (red).

and WIND. The hourly average SOHO velocity data show a good agreement during 7 November, up to 05:00 UT on 8 November, despite its large distance from ACE and WIND. After that, the SOHO velocity deviates significantly most of the time. It thus seems that the velocity structure is homogenous at the beginning of the period and then becomes more fragmented. The ACE and WIND densities show similar temporal variation, although WIND mostly gives higher densities, often by a factor 2 to 3. Except for the first part of 7 November, the SOHO density agrees quite well with the WIND density.

In Fig. 4 the crossing of the solar wind in the (Y, Z)-plane at X=10 R_E (typical megnetopause distance) is shown for the three spacecraft. As we only have all three velocity components for WIND, we have assumed the same velocity for the three spacecraft. The circle in the centre has a radius of 10 R_E. We see that the measurements at ACE advected to X=10 come reasonably close to the Earth during 7 November (dots). The most distant points are the two westerly dots, but simultaneously the WIND measurements come close to the Earth, and as ACE and WIND show a very good agreement for the whole period, we may conclude that the measurements at ACE depicts quite well what the solar wind is like close to the Earth during 7 November. Then, during 8 November, the advected location of ACE (diamonds) moves towards the east and south. During this day the velocities at SOHO and ACE also start to deviate. Then, during 9 November, the advected ACE location turns far south (crosses) of the Earth. It is thus possible that the measurements at ACE from the morning of 8 November through 9 November do not represent accurately the solar wind close to the Earth.

Turning back to the predictions shown in Figs. 2 and 3, it was seen that the correlation was higher during the first two days as compared to the last two days. Thus, this may be the result that the solar wind at ACE correlates well with the solar wind close to the Earth in the early part of the period but not later in the period. The errors are particularly large during the late evening to midnight on 9 November. Studying another model that predicts the geomagnetic index D_{st} (Lundstedt et al., 2002), also using ACE data as input, reveals that the prediction errors are large for the same hours.

4.2 The influence of B_z

Using the prediction models the influence of the solar wind on RMS ΔX and ΔY may be studied. In principal, some interesting artificial values could be selected to represent the solar wind to study the response of the model. However, care has to be taken so that the data represent a valid physical and statistical configuration, otherwise the output from the model will not be correct. One parameter that can be easily studied is B_z. It is perfectly valid to change the sign on B_z and run the models, as we expect that the direction of B is not correlated with density or velocity. For example, a magnetic cloud starts with a simultaneous increase in n, V, and B (Burlaga, 1995). But B_z may initially either turn northward or southward, with the subsequent evolution determined by the cloud topology. The result is shown in Fig. 5. The blue curve represents the original B_z and the red curve $-B_z$ (top panel). The model outputs are shown accordingly, in blue and red (bottom panels). The first apparent observation is that RMS ΔX shows a weak coupling to B_z, as changing the sign has very little effect on the output. On the contrary, RMS ΔY is much more affected.

Looking at the details we note that the variations in the two predictions of RMS ΔX are very similar up to 23:00 UT on 7 November, even though the sign on B_z has been changed. During the following hours, when B_z is strongly negative, up to 05:00 UT on 8 November there is a difference of about a factor 2. Then, the predictions coincide again when B_z goes towards zeros and the velocity decreases. But then, during a period of low activity from 12:00 UT on 8 November to 09:00 UT on 9 November, when B_z is close to zero, there is again a difference of a factor 2, with slightly higher activity when B_z is negative.

5 Conclusions

In this work we have studied the prediction of the 10-min variation of the local ground magnetic field, more specifically, the 10-min RMS ΔX and ΔY. The prediction model uses the solar wind data from the ACE spacecraft. The four-day period extending over 7 November to 10 November 2004 was explored.

It was found that the sample-to-sample variations in RMS ΔX and ΔY are not predicted, but the large-scale variations are predicted. The predictions of the first two days show a higher correlation with the observations than during the last two days. By studying the solar wind data for other L1-spacecraft (WIND and SOHO), it seems that the ACE data have a better agreement to the near-Earth solar wind during the first two days as compared to the last two days. In a study by Dalin et al. (2002) it was also shown that the correlation of solar wind plasma data from different spacecraft decreased with increasing (Y, Z)-separation. Thus, the accuracy of the predictions depends on the location of the spacecraft and the solar wind flow direction.

The models have not been developed to predict the response of ΔX or ΔY for specific solar wind structures; the only criterion used on the data selection is that there should be contiguous data for 48 h, or longer, for which RMS >10 nT/min at least once. This means that solitary peaks in RMS ΔX or ΔY will be difficult to model because of the low relative occurrence rate. However, the peaks may also be related to magnetic impulse events (Kataoka et al., 2003) that show a significant correlation to discontinuities of the interplanetary magnetic field, and not B_z, therefore, additional inputs should be considered in future studies.

By modifying the solar wind input data the response of the model may be studied. Care has to be taken in how the input is modified, but a valid modification from a physical and statistical point of view is to change the sign of B_z. It was found, for the events studied here, that the ΔX and ΔY models showed a very different dependence on B_z. The ΔX model is almost independent of the solar wind magnetic field B_z, except at times when B_z is large or when the overall activity is low. On the contrary, the ΔY model shows a strong dependence on B_z at all times.

In the models developed by Wintoft (2005) the location of ACE was not considered. Thus, it is reasonable to believe that there are data in the solar wind data set used for model development that are poorly correlated to the near-Earth solar wind. The inclusion of such data during the model development has the effect of increased noise. In future work, a more careful selection of data, taking into account the location of ACE, should be considered.

Acknowledgements. We are grateful to the providers of the solar wind and ground magnetic field data: ACE data from CalTech and SEC; the MIT Space Plasma Group for the WIND plasma data and NASA/GSFC for the WIND magnetic field data; the University of Maryland for the SOHO/PM data; the Solar-Terrestrial Physics Division at the Danish Meteorological Institute for the Brorfelde magnetic field data. COST 724 is acknowledged for financial support. This work has been carried out with support from ESA/ESTEC (Contract No. 16953/02/NL/LvH).

Topical Editor T. Pulkkinen thanks J. B. Blake and another referee for their help in evaluating this paper.

References

Baker, D. N.: Statistical analyses in the study of solar wind-magnetosphere coupling, Solar Wind-Magnetosphere Coupling, 17–38, 1986.

Baumjohann, W. and Haerendel, G.: Entry and dissipation of energy in the Earth's magnetosphere, in Space Astronomy and Solar System Exploration: Proceeding of summer school held at aplbach, Austria, 29 July–8 August, 1986, 121–130, ESA, 1987.

Boberg, F., Wintoft, P., and Lundstedt, H.: Real time K_p predictions from solar wind data using neural networks, Physics and Chemistry of the Earth, 25, 275–280, 2000.

Boteler, D.: Assessment of geomagnetic hazards to power systems in Canada, Natural Hazards, 23, 101–120, 2001.

Boteler, D. H., Pirjola, R. J., and Nevanlinna, H.: The effects of geomagnetic disturbances on electrical systems at the Earth's surface, Adv. Space Res., 22, 17–27, 1998.

Burlaga, L. F.: Interplanetary magnetohydrodynamics, Oxford University Press, 1995.

Dalin, P., Zastenker, G., Paularena, K., and Richardson, J.: The main features of solar wind plasma correlations of importance to space weather strategy, J. Atmos. S.-P., 64, 737–742, 2002.

Detman, T. R. and Vassiliadis, D.: Review of techniques for magnetic storm forecasting, 253–266, AGU, 1997.

Echer, E. and Gonzales, W. D.: Geoeffectiveness of interplanetary shocks, magnetic clouds, sector boundary crossings and their combined occurrence, Geophys. Res. Lett., 31, L09 808, 2004.

Gleisner, H. and Lundstedt, H.: Auroral electrojet predictions with dynamic neural networks, J. Geophys. Res., 106, 24 541–24 550, 2001a.

Gleisner, H. and Lundstedt, H.: Neural network-based local model for prediction of geomagnetic disturbances, J. Geophys. Res., 106, 8425–8433, 2001b.

Gonzalez, W. D., Joselyn, J. A., Kamide, Y., Kroehl, H. W., Rostoker, G., Tsurutani, B. T., and Vasyliunas, V. M.: What is a geomagnetic storm?, J. Geophys. Res., 99, 5771–5792, 1994.

Gosling, J. T., McComas, D. J., Phillips, J. L., and Bame, S. J.: Geomagnetic activity associated with Earth passage of interplanetary shock disturbances and coronal mass ejections, J. Geophys. Res., 96, 7831–7839, 1991.

Huttunen, K. E. J., Koskinen, H. E. J., and Schwenn, R.: Variability of magnetospheric storms driven by different solar wind pertubations, J. Geophys. Res., 107, SMP 20–1–8, 2002.

Ipavich, F. M., Galvin, A. B., Lasley, S. E., Paquette, J. A., Hefti, S., Reiche, K., Coplan, M. A., Gloeckler, G., Bochsler, P., Hovestadt, D., Grünwaldt, H., Hilchenbach, M., et al.: Solar wind measurements with SOHO: The CELIAS/MTOF proton monitor, J. Geophys. Res., 103, 17 205–17 213, 1998.

Kataoka, R., Fukunishi, H., and Lanzerotti, L. J.: Statistical identification of solar wind origins of magnetic impulsive events, J. Geophys. Res., 108, SMP 13–1–12, 2003.

Klimas, A. J., Vassiliadis, D., and Baker, D. N.: D_{st} index prediction using data-derived analogues of the magnetospheric dynamics, J. Geophys. Res., 103, 20 435–20 448, 1998.

Lundstedt, H., Gleisner, H., and Wintoft, P.: Operational forecasts of the geomagnetic *Dst* index, Geophys. Res. Lett., 29, 34–1–34–4, 2002.

Mayaud, P. N.: Derivation, meaning, and use of geomagnetic indices, Geophysical Monograph Series, AGU, 1980.

McComas, D. J., Bame, S. J., Barker, P., Feldman, W. C., Phillips, J. L., Riley, P., and Griffee, J. W.: Solar wind electron proton alpha monitor (SWEPAM) for the Advanced Composition Explorer, Space Science Reviews, 86, 563–612, 1998.

Nishida, A.: Geomagnetic Diagnosis of the Magnetosphere, 9 of Physics and Chemistry in Space, Springer-Verlag, 1978.

Ogilvie, K. W., Chornay, D. J., Fritzenreiter, R. J., Hunsaker, F., Keller, J., Lobell, J., Miller, G., Scudder, J. D., Sittler, Jr., E. C., Torbert, R. B., Bodet, D., Needell, G., Lazarus, A. J., et al.: SWE, a comprehensive plasma instrument for the WIND spacecraft, Sp. Sc. R., 71, 55–77, 1995.

Owens, M. J., Cargill, P. J., Pagel, C., Siscoe, G. L., and Crooker, N. U.: Characteristic magnetic field and speed properties of interplanetary coronal mass ejections and their sheath regions, J. Geophys. Res., 110(A01), 105, 2005.

Percival, D. B. and Walden, A. T.: Wavelet methods for time series analysis, Cambridge University Press, 2002.

Pirjola, R.: Review on the calculation of surface electric and magnetic fields and of geomagnetically induced currents in ground-based technological systems, Surv. Geophys., 23, 71–90, 2002.

Richardson, I. G., Cane, H. V., and Cliver, E. W.: Sources of geomagnetic activity during nearly three solar cycles, J. Geophys. Res., 107, SSH 8–1–13, 2002.

Smith, C. W., L'Heureux, J., Ness, N. F., Acuña, M. H., Burlaga, L. F., and Scheifele, J.: The ACE magnetic fields experiment, Space Sci. R., 86, 613–632, 1998.

Vassiliadis, D. and Klimas, A. J.: The $D_s t$ geomagnetic response as a function of storm phase and amplitude and the solar wind electric field, J. Geophys. Res., 104, 24 957–24 976, 1999.

Viljanen, A., Nevanlinna, H., Pajunpää, K., and Pulkkinen, A.: Time derivate of the horizontal geomagnetic field as an activity indicator, Ann. Geophys., 19, 1107–1118, 2001,
SRef-ID: 1432-0576/ag/2001-19-1107.

Viljanen, A., Pulkkinen, A., Amm, O., Pirjola, R., Korja, T., and BEAR Working Group: Fast computation of the geoelctric field using the method of elementary current systems and planar Earth models, Ann. Geophys., 22, 101–113, 2004,
SRef-ID: 1432-0576/ag/2004-22-101.

Weigel, R. S., Vassiliadis, D., and Klimas, A. J.: Coupling of the solar wind to temporal fluctuations in ground magnetic fields, Geophys. Res. Lett., 29, 2002.

Wintoft, P.: Study of the Solar Wind Coupling to the Time Difference Horizontal Geomagnetic Field, Ann. Geophys., 23, 1949–1957, 2005,
SRef-ID: 1432-0576/ag/2005-23-1949.

Wu, J.-G. and Lundstedt, H.: Neural network modeling of solar wind–magnetosphere interaction, J. Geophys. Res., 102, 14 457–14 466, 1997.